MDPI

Article

Role of Al in the Solution Strengthening of Mg–Al Binary Alloys

Tingting Liu [1,*] **, Yanglu Liu** [2,3] **, Lu Xiao** [2] **, Shibo Zhou** [2] **and Bo Song** [1,*]

[1] School of Materials and Energy, Southwest University, Chongqing 400715, China
[2] Materials Science and Engineering College, Chongqing University, Chongqing 400044, China;
    wewewe-12345@163.com (Y.L.); L_Xiao@cqu.edu.cn (L.X.); zhoushibo1994@foxmail.com (S.Z.)
[3] Patent Examination Cooperation Sichuan Center of the Patent Office, CNIPA, Chengdu 610213, China
* Correspondence: ttliu@swu.edu.cn (T.L.); bosong@swu.edu.cn (B.S.)

Abstract: Mg–Al binary alloys in the concentration range from 0 to 4.0 wt.% Al have been prepared under conventional casting conditions. The as-cast Mg and Mg–Al alloys after solution treatment were processed via hot extrusion at 350 °C. The results show that Al has a positive influence on grain refinement and solution strengthening. The as-extruded Mg–Al alloys are fully recrystallized, and the tensile yield strength of the binary alloys is two times higher than that of pure Mg. Furthermore, the elongations of Mg–Al alloys are much higher than that of pure Mg. In addition, Mg and Mg–Al alloys were further studied by the viscoplastic self-consistent (VPSC) model to explore the activation and evolution of deformation modes. The simulation results match well with the experimental results.

Keywords: magnesium; alloying element; solution strengthening; viscoplastic self-consistent model

1. Introduction

As the lightest structural metallic material, magnesium has much wide application prospect, because of its good castability, good machinability, good electromagnetic shielding capability, good weldability and so on. It is known that the application of Mg alloys would be more extensive if they have good plastic deformability [1].

Adding alloying elements to pure magnesium can make a significant improvement, so that magnesium alloys are provided with various properties to meet different requirements [2,3]. Aluminum is the commonly used alloying element to improve the mechanical properties, enhance die castability and corrosion resistance of magnesium alloys [4,5]. Al in Mg alloys has two existence forms: one exists in $Mg_{17}Al_{12}$ phases, the other solubilizes in the Mg matrix. Usually, the addition of Al leads to obvious grain refinement for Mg alloys, because the aluminum compound particles are the active heterogeneous nucleation sites for the Mg matrix [6,7]. Generally, $Mg_{17}Al_{12}$ phases can significantly affect the corrosion, wear and mechanical properties of Mg–Al alloys [8–10]. Many studies show that the existence of $Mg_{17}Al_{12}$ precipitates has a great influence on the grain structure during thermal deformation, thus affecting the strength of the deformed alloy [11–14]. However, the effect of Al atoms solid solution in Mg on the mechanical properties and deformation behavior of magnesium alloys is rarely studied.

Recently, more and more researchers have paid attention to the study of deformation mechanisms and the parameters that affect the mechanical properties that could be analyzed by means of the simulation method [15–19]. The viscoplastic self-consistent (VPSC) model is a powerful tool to predict texture evolution and macroscopic plastic of polycrystalline aggregates, which is widely applied for hcp metal, especially for Mg alloys [20]. The VPSC model was originally due to Molinari et al. [21] and extended to fully anisotropic behavior and comprehensive derivations by Lebensohn and Tomé [22,23]. Many researchers discussed the plastic deformation and evolution of texture of Mg–Y, Mg–Gd, AZ31, ZK60

and other Mg alloys by VPSC modeling [24–26]. These studies showed that the simulated results were in good agreement with the measurement.

In this work, the microstructure and mechanical properties of Mg–Al solid solution alloys with different Al concentrations were investigated. Furthermore, we utilized VPSC simulation to investigate the deformation behaviors of the binary alloys in order to explain the effect of Al in solid solution on the deformation mechanism of Mg–Al alloys.

2. Materials and Methods

The Mg–xAl (x = 1, 2, 3, 4) alloys were prepared from pure commercial Mg (>99.97 wt.%) and pure Al (>99 wt.%) by an electric resistance furnace under the protective of a gas mixture of CO_2 and SF_6 at 730 °C. Then, the melt was poured into a steel mold with cylindrical cavity of 100 mm in diameter and 150 mm in height, which preheated 320 °C. The chemical composition of the samples was analyzed by X-ray Fluorescence (Shimadzu XRF-1800, Shimadzu, Japan), and the results were given in Table 1. The as-cast Mg–Al alloys were homogenized at 420 °C for 20 h and cooled in air. The billets were preheated to 300 °C for 1 h and extruded by a XJ-500 Horizontal Extrusion Machine (Yuanchang Machinery, Wuxi, China) made in China at a constant force. Solid rods are approximately 16 mm in diameter, corresponding to the extrusion ratio of 25:1 and the speed was 1 mm/min and air-cooled. Afterward, the tensile specimens of as-extruded rods along the extrusion direction were machined with 5 mm in diameter and 25 mm in length in the gauge section.

Table 1. Compositions and mechanical properties of the as-extruded Mg–Al alloys.

Alloys	Compositions (wt.%)	TYS (MPa)	UTS (MPa)	FE (%)
Mg	Mg	75 ± 0.5	182 ± 0.8	15.1 ± 0.2
Mg–1Al	Mg–1.06Al	142 ± 1.7	225 ± 1.2	17.1 ± 0.6
Mg–2Al	Mg–1.99Al	151 ± 0.9	230 ± 0.9	20.4 ± 0.8
Mg–3Al	Mg–3.07Al	156 ± 0.8	240 ± 0.5	21.3 ± 0.9
Mg–4Al	Mg–3.96Al	160 ± 1.2	251 ± 0.8	20.8 ± 0.9

The microstructure of solution-treated samples and the untreated ones were observed with a scanning electron microscope (SEM, Tescan Vega II, Czech Republic). Phases and texture analysis of as-extruded alloys was carried out on a transverse section by X-ray diffraction with a Cu target (XRD, D/MAX-2500PC, Rigaku, Tokyo, Japan). The measurement angular range of phases analysis was from 20° to 90°, and the angular step was 1.0°/min. An optical microscope (OM, Zeiss Axio Observer A1, Zeiss, Germany) was used to observe the microstructure of the extruded samples on the longitudinal section. The metallographic samples for OM and SEM observations were firstly ground with SiC papers, flowed by chemically etched in alcohol nitrate solution for ~20 s. The grain size was measured by the linear intercept method using OM images. EBSD analysis was carried out in a SEM (JEOL JSM-7800F, Tokyo, Japan) equipped with an Oxford Instruments NordlysNano EBSD detector using Aztec and Channel software to collect and analyzed data. Besides, EBSD was performed at 20 KV, 14 mm working distance, 70° tilt and 0.8–1.0 μm scan steps.

To investigate the mechanical properties at room temperature, the samples were pulled to failure in a universal testing machine (CMT5105) at a constant strain rate of 1×10^{-3} s^{-1}. The results of ultimate tensile strength (UTS), tensile yield strength (TYS, offset = 0.2%) and elongation of fracture (FE) were the average value measured at least three specimens from different location of the extruded rods. The deformation behavior during tensile deformation is analyzed by VPSC modeling. The interaction between grains in polycrystal was taken into account in the model; each grain is treated as an ellipoisal viscoplastic inclusion embedded in an effective viscoplastic medium. The viscoplastic constitutive behavior was described by means of the nonlinear rate-sensitivity equation [21–23]:

$$\varepsilon_{ij}(\overline{x}) = \sum_s m_{ij}{}^s \gamma^s(\overline{x}) = \gamma_0 \sum_s m_{ij}{}^s \left\{ \frac{m_{kl}{}^s \sigma_{kl}(\overline{x})}{\tau_s} \right\} \tag{1}$$

In the above expression τ_s and $m_{ij}{}^s$ were the threshold stress and the symmetric Schmid tensor associated with slip (or twin) systems; $\varepsilon_{ij}(\overline{x})$ and $\sigma_{kl}(\overline{x})$ were the deviatoric strain-rate and stress; $\gamma^s(\overline{x})$ was the local shear-rate on slip systems. It was characterized by an evolution of the threshold stress with accumulated shear strain in each grain of the form:

$$\tau^s = \tau_0{}^s + (\tau_1{}^s + \theta_1{}^s \Gamma)\left(1 - \exp\left(-\Gamma \left| \frac{\theta_0{}^s}{\tau_1{}^s} \right| \right) \right) \tag{2}$$

In this formula $\Gamma = \sum_s \Delta\gamma^s$ was the accumulated shear in the grain; τ_0, $(\tau_0 + \tau_1)$, θ_0, θ_1 were the initial CRSS, the back-extrapolated CRSS, the initial hardening rate and the asymptotic hardening rate.

3. Results and Discussion

The SEM micrographs of the as-cast Mg–Al alloy and the solid solution alloys are shown in Figure 1. According to Mg–Al binary phase diagram, aluminum can form the finite solid solution with Mg, while the maximum solubility is about 2 wt.% at room temperature [27]. According to Figure 1a,c,e,g, there are a few second phases in the Mg–Al alloy when the concentration of Al is under 2 wt.%. With the increase of Al concentration, the number of second phase particles increases, and the size of second phase particles becomes bigger. To figure out the second phase, detailed views of the as-cast Mg–4Al alloy are shown in Figure 2. According to the energy dispersive spectroscopy (EDS) results, the dark field (A) is the Mg matrix; the bright lumps (B) and particles (C) consist of magnesium and aluminum, which should be β-$Mg_{17}Al_{12}$. A comparison of the untreated (Figure 1a,c,e,g) with homogenized samples (Figure 1b,d,f,h) indicates that the second phases are nearly dissolved into the matrix within the four different samples at 420 °C after heat-treatment of the solid solution.

Figure 3a shows XRD patterns of Mg and solution-treated Mg–Al alloys. Only Mg is detected in the patterns. Peaks of Mg are in agreement with the standard pattern (PDF #65-3365) [28]. Figure 3b shows the comparison of XRD patterns between as-cast and solution-treated Mg–4Al alloy. It can be seen that there are some $Mg_{17}Al_{12}$ phases in as-cast Mg–4Al alloy. After heat treatment, $Mg_{17}Al_{12}$ phases are dissolved in Mg matrix and peaks of solution treated Mg–4Al alloy deviate from the standard pattern to small angle. According to Bragg equation, the diffraction peaks shift a little to the right, which means the diffraction angle (θ) increases and the crystalline interplanar spacing (d) decreases correspondingly. The phenomenon reveals that some locations of Mg have been taken up by smaller atoms (Al), which leads to the change in the crystalline structure. As is known to all, lattice distortion will affect the properties of Mg alloys, such as the improvement of yield strength [29,30].

The OM images in Figure 4a–e show the longitudinal-sectional microstructure evolution of extruded Mg–Al alloys. As demonstrated in Figure 4a, the as-extruded Mg exhibited a partly recrystallized grain size of 35.3 ± 8.2 µm even though it has a minority of elongated grains along the extrusion direction. The average grain size of Mg–xAl (x = 1, 2, 3, 4) alloys are 24.3 ± 6.8 µm, 20.3 ± 5.6 µm, 17.7 ± 4.8 µm and 16.6 ± 4.1 µm, respectively. It can be seen that Al has a positive influence on grain refinement, and grain size is related to the Al concentration. However, there is little difference in grain size between Mg–3Al alloy (Figure 4d) and Mg–4Al alloy (Figure 4e), and it implies that the average grain size won't change significantly when the concentration of Al is more than 3 wt.%. Figure 4f shows the SEM image obtained from Mg–4Al alloy, and the EDS results show that most of Al are dissolved in the Mg matrix.
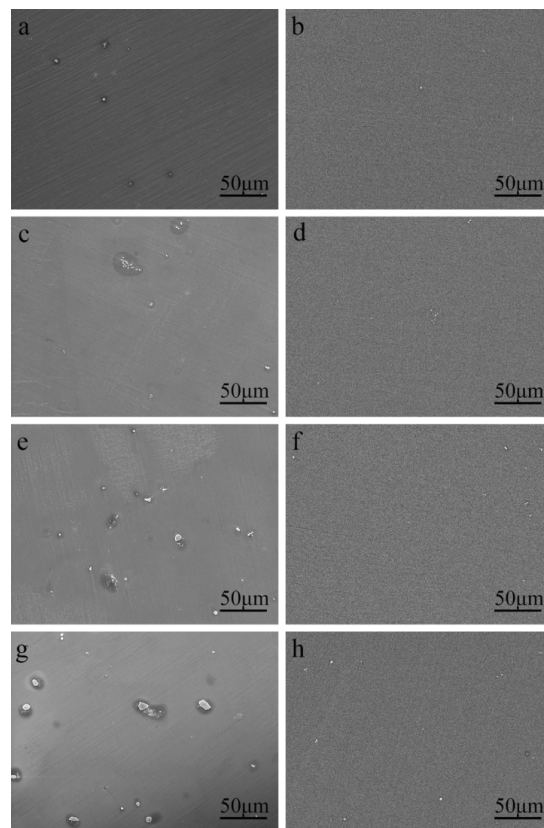
Figure 1. SEM micrographs of (**a**,**c**,**e**,**g**) as-cast Mg–xAl (x = 1, 2, 3, 4) alloys and (**b**,**d**,**f**,**h**) solution treated Mg–xAl (x = 1, 2, 3, 4) alloys.
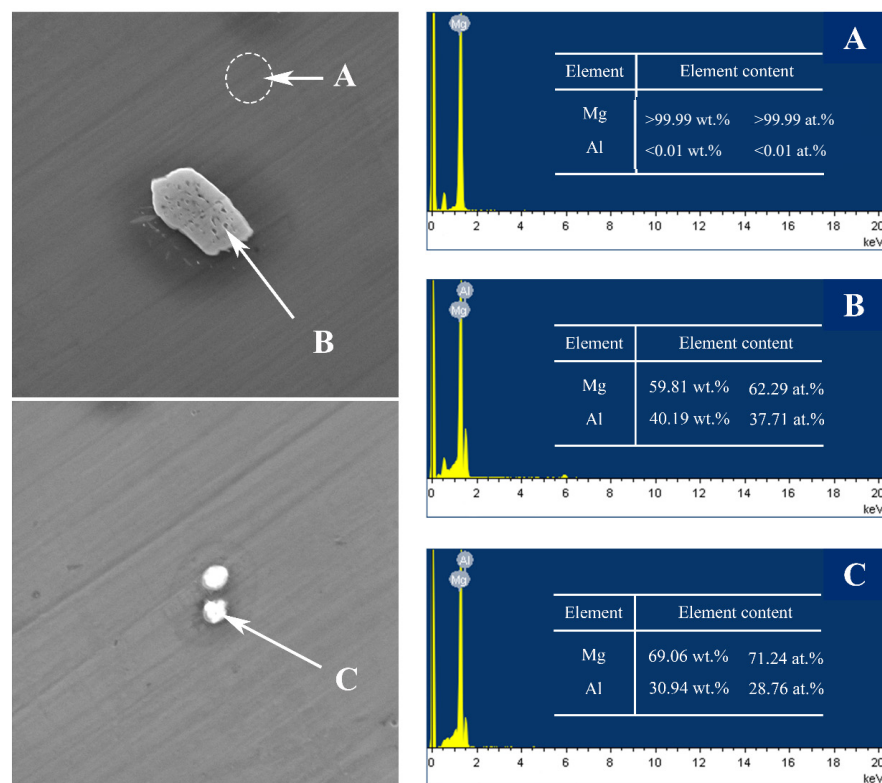

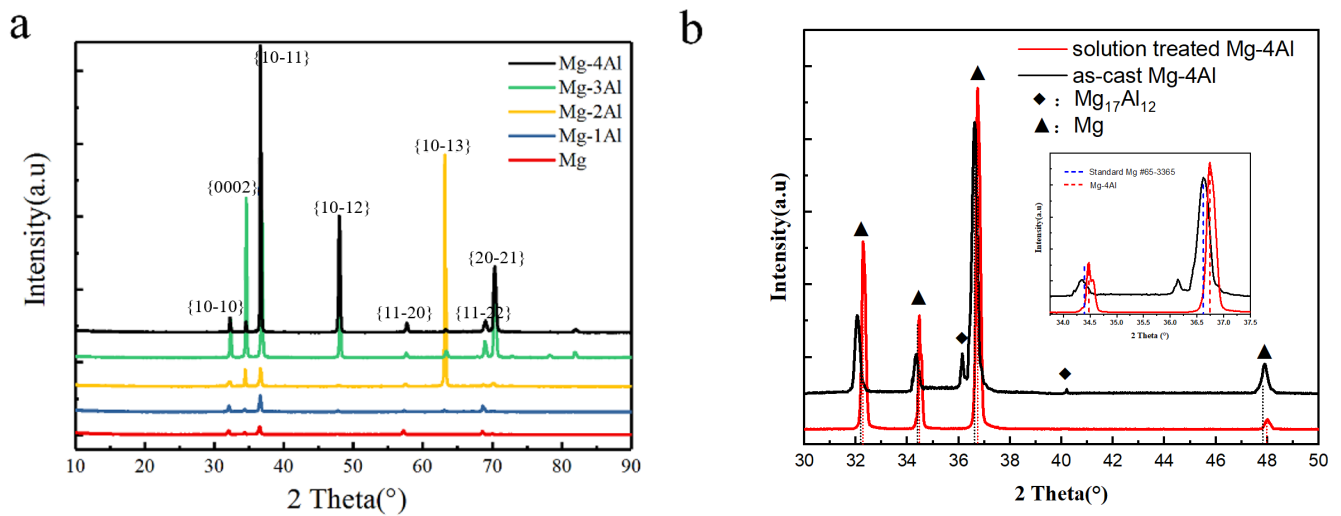**Figure 2.** SEM micrographs and corresponding EDS results of as-cast Mg–4Al alloy at different position (**A–C**).

Figure 3. XRD patterns of (**a**) the solution treated Mg–Al alloys with different Al content, (**b**) as-cast and solid treated Mg–4Al alloy.
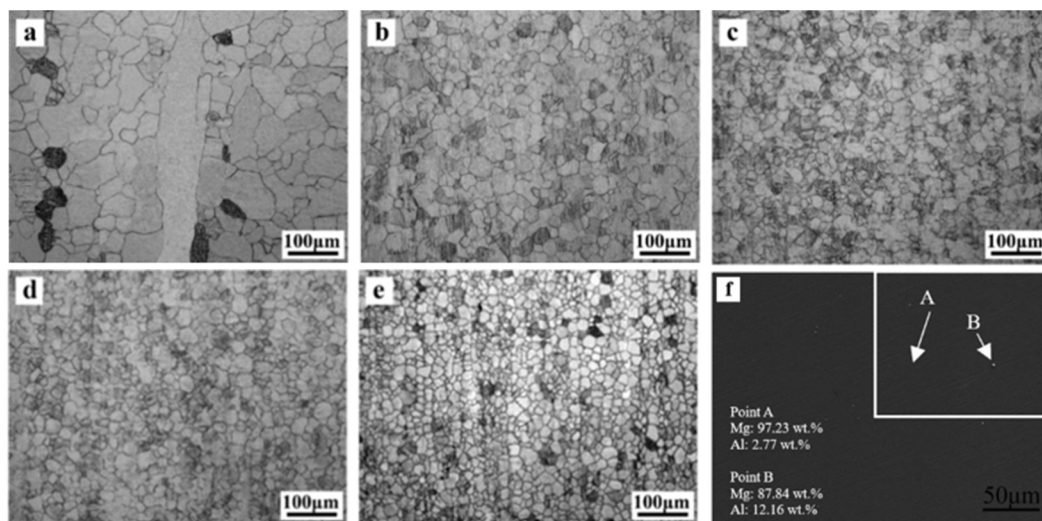

Figure 4. Optical microscope images of the as-extruded Mg–Al alloys with different Al content along the extrusion direction: (**a**) Mg, (**b**) Mg–1Al, (**c**) Mg–2Al, (**d**) Mg–3Al, (**e**) Mg–4Al, and (**f**) SEM image obtained from Mg–4Al alloy.

Figure 5 shows the actual stress–strain curves, and mechanical properties of Mg and Mg–Al alloys at room temperature are listed in Table 1. Tensile yield strength (TYS), ultimate tensile strength (UTS) and fracture elongation (FE) of Mg are 75 MPa, 182 MPa and 15.1%, respectively. Meanwhile, these properties of Mg–Al alloys are all improved remarkably. What's more, for Mg–xAl (x = 1, 2, 3, 4) alloys, yield strength increases from 142 MPa to 160 MPa, and ultimate tensile strength rises from 225 MPa to 251 MPa. And the fracture elongation of Mg–3Al reaches the maximum of 21.3% among four Mg–Al alloys. The yield strength of all Mg–Al alloys is nearly twice as much as Mg. However, continuing to add aluminum cannot improve the properties sharply. This variation tendency goes along with the mechanical testing results of as-cast Mg–6Zn alloy, of which tensile properties are gradually improved within the range of 0~3% Al [25]. In other words, the solid solution of Al has a favorable effect on mechanical properties of pure Mg.
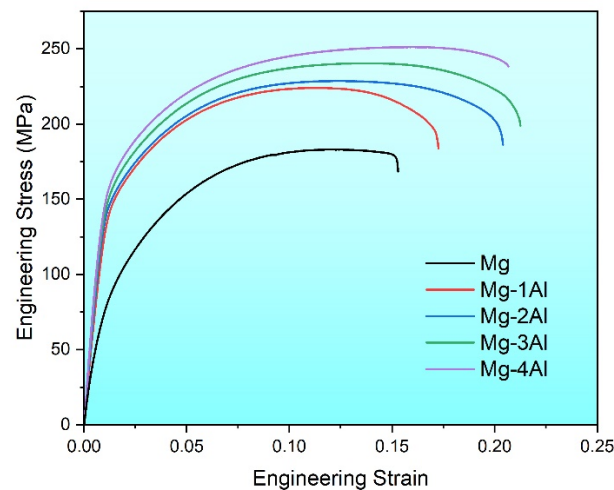
Figure 5. Tensile stress–strain curves of the as-extruded Mg–xAl (x = 0, 1, 2, 3, 4) alloys.

The EBSD results (inverse pole figure (IPF) maps) obtained from the cross section of the alloy are shown in Figure 6. It is shown that grains of Mg and Mg–Al alloy have the similar orientation by the color distribution in IPF maps. In these system alloys, green zone illustrated that the grain is orientated with ($10\bar{1}0$) plane and blthe ue zone represents ($11\bar{2}0$) plane. That is to say, the as-extruded samples present a basal texture that the basal planes of most grains parallel to the extrusion direction. Still, small variation goes forward along with the concentration, the region of green and blue trends to narrow down slightly, which illustrates that the addition of Al modifies the grain orientation in Mg–Al alloy and weaken the texture.
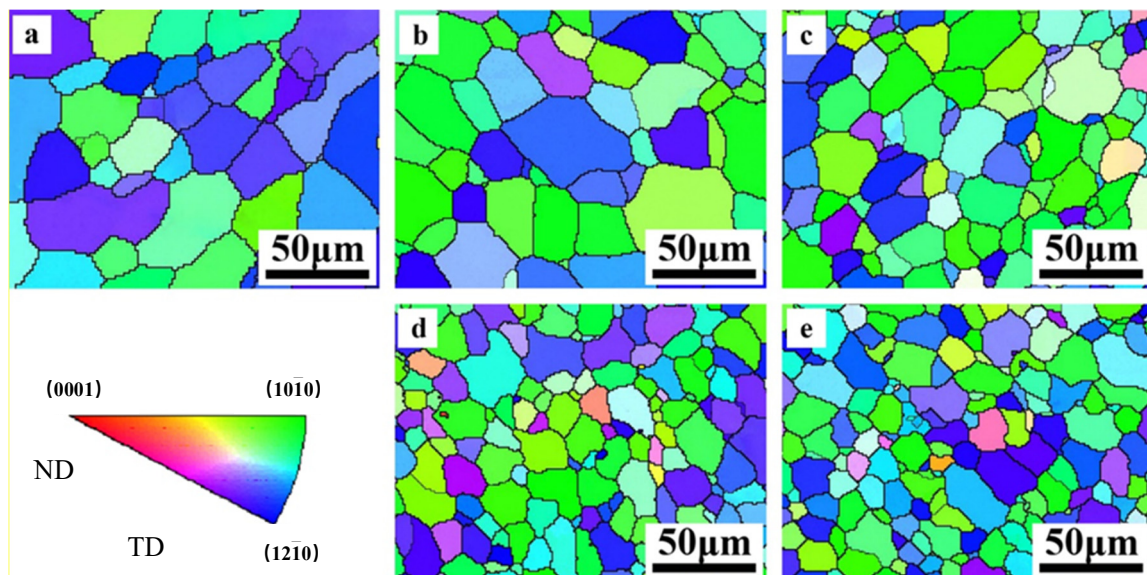

Figure 6. EBSD of as-extruded Mg–Al alloy (**a**) Mg, (**b**) Mg–1Al, (**c**) Mg–2Al, (**d**) Mg–3Al, (**e**) Mg–4Al.

Figure 7 is pole figures to show the texture of the cross-sectional as-extruded alloys measured by XRD. Most hcp materials present a basal texture around the extrusion axis which is developed during uni-axial deformation, and it is also commonly observed after round extrusion of wrought magnesium alloys. Mg and Mg–Al alloys show a typical ring fiber texture according to the graphs. The maximum value of texture intensities of Mg–xAl (x = 0, 2, 4) alloys are 4.2 multiples of random distribution (m.r.d), 3.1 m.r.d, 3.1 m.r.d, respectively. Coinciding with EBSD analysis, it indicates that the addition of Al

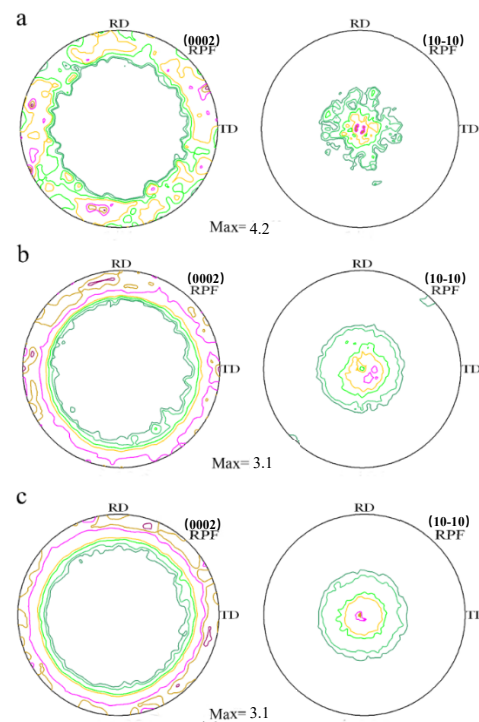has a tendency to weaken basal texture, which could benefit the elongation of alloys at room temperature.

Figure 7. Pole figure of as-extruded Mg–Al alloys measured by X-ray diffraction: (**a**) Mg, (**b**) Mg–2Al, (**c**) Mg–4Al.

Strong basal texture of Mg alloys leads to higher tensile yield strength due to the activity of basal slip, which requires higher shear stress [31–33]. On the contrary, some alloying elements [30,31], such as Al can weaken basal texture based on Figure 7. Generally, if tension stress along the extrusion direction is applied on the samples as investigated in this paper, basal slip of Mg–Al alloys will be prone to be activated compared with Mg, then Mg–Al alloys would suffer a loss of yield strength. However, the yield strengths of Mg–Al alloys do not decrease but increase, which should be influenced by other strengthening mechanisms. According to Hall–Patch relationship [34], it's found that the coefficient of Hall–Patch is 180 MPaμm$^{1/2}$ when the grain size is about 20 μm. In this work, the strength contribution from grain boundaries of Mg–xAl (x = 1, 2, 3, 4) alloys is 37 MPa, 40 MPa, 43 MPa and 44 MPa, respectively. Combining with the consequence of Figure 3, most of Al atoms dissolve in the Mg matrix, resulting in solid solution strengthening. Therefore, Mg–Al alloys show higher yield strength than Mg under the same extrusion condition. And it also can be seen that texture strengthening is not the main strengthening mechanism in this work. In addition, the ductility of Mg–Al alloys increases with the increase of Al content from 1 wt.% to 3 wt.%, which is mainly caused by grain refinement.

VPSC simulation is applied to making a further investigation of the deformation behavior of Mg–Al alloys. Polycrystal used in this simulation consists of about 8000 grains with various orientations, and the initial texture is obtained from XRD results. Six deformation modes are simulated during the process, which include basal <a> slip ({0001}<11$\bar{2}$0>), prismatic <a> slip ({10$\bar{1}$0}<11$\bar{2}$0>), pyramidal <a> slip ({10$\bar{1}$1}<11$\bar{2}$0>), pyramidal <c + a> slip ({11$\bar{2}$2}<11$\bar{2}$3>), {10$\bar{1}$2}<10$\bar{1}$1> extension twins and {10$\bar{1}$1}<10$\bar{1}$2> contraction twins. Combining with tensile test of Mg–Al alloys at room temperature, the hardening parameters of Mg–Al alloys are obtained by numerical fitting, which are displayed in Table 2. Experimental and simulated results of strain-stress curves are shown in Figure 8. It is observed that the calculated results are in good agreement with experimental data.

Table 2. Parameters for VPSC constitutive model of Mg–xAl (x = 0, 2, 4) alloy.

| Specimens	Mode	τ_0/MPa	τ_1/MPa	θ_0/MPa	θ_1/MPa
	Basal	5	30	800	30
	Prismatic	150	10	1200	0
Mg	Pyramidal <a>	245	10	300	0
	Pyramidal <c + a>	185	10	100	0
	Extension twin	80	100	2500	0
	Contraction twin	275	300	1500	0
	Basal	18	30	1000	70
	Prismatic	180	10	1200	0
Mg–2Al	Pyramidal <a>	245	65	300	0
	Pyramidal <c + a>	205	70	100	0
	Extension twin	75	170	2500	0
	Contraction twin	275	300	1500	0
	Basal	22	30	1000	80
	Prismatic	200	10	1200	0
Mg–4Al	Pyramidal <a>	245	65	300	0
	Pyramidal <c + a>	225	70	100	0
	Extension twin	70	170	2500	0
	Contraction twin	275	300	1500	0
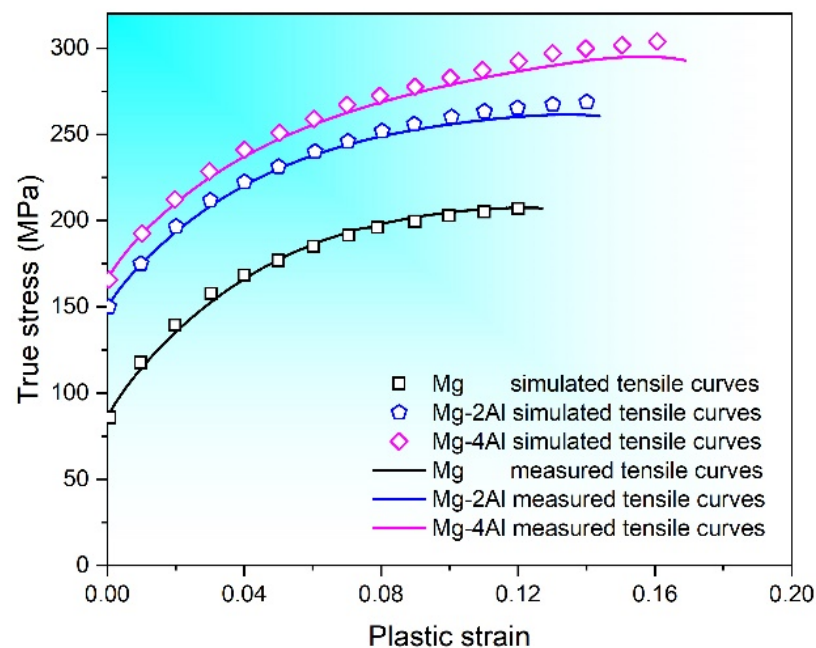
Figure 8. Measured and simulated flow curves for Mg–xAl (x = 0, 2, 4) alloys.

Figure 9 is the relative activity of deformation behavior. According to the curves, relative activities change with the increase of plastic strain. Figure 9a illustrates that basal slip is the overriding deformation mode in Mg. In Figure 9b,c, at the beginning of tensile process, deformation modes of Mg–Al alloys are given priority to with basal slip, while extension twins are the auxiliary deformation mode. Besides, the relative activity of extension twins increases from 0 to 0.05, even it fades away soon, and the prismatic slip starts immediately. When strain comes to 3%, prismatic slip mainly replaces extension twins. Afterward, prismatic slip shows an increasing tendency which makes basal slip come down at the same time. At the end of the plastic tensile test, relative activity of prismatic slip rises to 0.22 and 0.35 in Mg–2Al alloy and Mg–4Al alloy respectively, while basal slip falls to 0.76 and 0.62. In a word, the simulation results show that basal slip plays a decisive part in the deformation mechanism in Mg, while the activations of extension twins and prismatic slip in Mg–Al alloys are promoted at different stages with Al concentration.

Pyramidal slip and contraction twins are extremely difficult to be activated during the tensile process. Investigations show that basal <a> slip is the dominating deformation mechanism and the CRSS of basal slip is about 0.45~0.81 MPa [35,36]. The secondary slip is prismatic <a> slip, of which CRSS is near 39.2 MPa and the CRSS of pyramidal slip is much higher comparatively. Thus, basal slip is the easiest deformation mode than other slips and twins. Reviewed the analysis of tensile test and the relative activities of deformation modes, the addition of Al can promote the activation of extension twins and reduce the activity of basal slip at the beginning of the tensile test. In addition, because the CRSS of extension twins is higher than that of basal slip, more activation of extension twins needs higher applied stress, then yield strength of the Mg–Al alloys would be improved. It is worth noting that the increasing prismatic slip replaces some basal slip during the later tensile deformation. The activation of prismatic slip is promoted to accommodate basal slip probably.
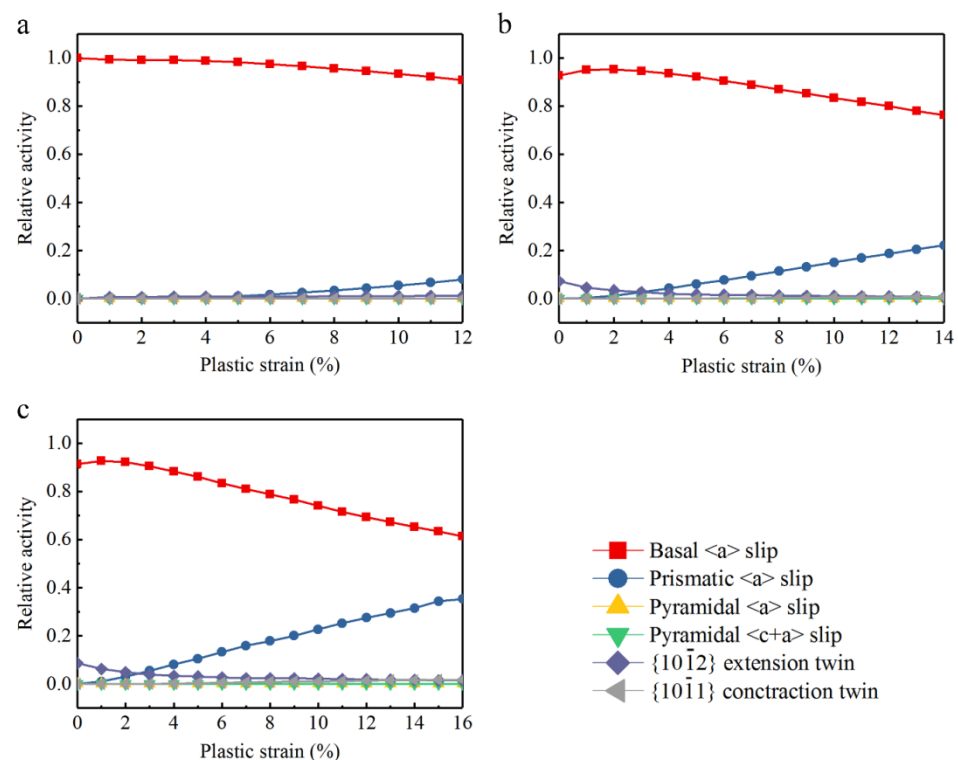

Figure 9. Simulated relative activity of deformation modes: (**a**) Mg, (**b**) Mg–2Al, (**c**) Mg–4Al.

4. Conclusions

The microstructure and mechanical properties of Mg and Mg–Al alloys have been investigated in this paper. The major conclusions are as follows:

1. Microstructure of as-extruded Mg–Al alloys has been refined and the average grain size is related to the concentration of aluminum within certain limits. Moreover, the texture of as-extruded Mg–Al alloys is in a similar situation as well.

2. For Mg–xAl (x = 1, 2, 3, 4) alloys, yield strength increases from 142 MPa to 160 MPa, and ultimate tensile strength rises from 225 MPa to 251 MPa. And the fracture elongation of Mg–3Al reaches the maximum of 21.3% among four Mg–Al alloys.

3. The results of VPSC simulation match well with the experimental data. The simulation results show that basal slip plays a decisive part in deformation mechanism in Mg alloys.

5. Patents

This section is not mandatory but may be added if there are patents resulting from the work reported in this manuscript.

References

1. Alanem, K.K.; Okotete, E.A. Enhancing plastic deformability of Mg and its alloys—A review of traditional and nascent developments. *J. Magnes. Alloy.* **2017**, *5*, 460–475. [CrossRef]
2. Song, J.F.; She, J.; Chen, D.L.; Pan, F.S. Latest research advances on magnesium and magnesium alloys worldwide. *J. Magnes. Alloy.* **2020**, *8*, 1–41. [CrossRef]
3. Gu, D.D.; Peng, J.; Wang, J.W.; Liu, Z.T.; Pan, F.S. Effect of Mn Modification on the Corrosion Susceptibility of Mg–Mn Alloys by Magnesium Scrap. *Acta Metall. Sinica* **2021**, *34*, 1–11. [CrossRef]
4. Liao, H.B.; Zhan, M.Y.; Li, C.B.; Ma, Z.Q.; Du, J. Grain refinement of Mg–Al alloys inoculated by $MgAl_2O_4$ powder. *J. Magnes. Alloy.* **2021**, *9*, 1211–1219. [CrossRef]
5. Mordike, B.L.; Ebert, T. Thermal conductivity of as-cast and as-extruded binary Mg–Al alloys. *J. Alloy. Compd.* **2014**, *608*, 19–24.
6. Wang, C.L.; Dai, J.C.; Liu, W.C.; Zhang, L.; Wu, G.H. Effect of Al additions on grain refinement and mechanical properties of Mg-Sm alloys. *J. Alloy. Compd.* **2015**, *620*, 172–179. [CrossRef]
7. Jiang, Z.T.; Jiang, B.; Yang, H.; Yang, Q.S.; Dai, J.H.; Pan, F.S. Influence of the Al_2Ca phase on microstructure and mechanical properties of Mg–Al–Ca alloys. *J. Alloy. Compd.* **2015**, *647*, 357–363. [CrossRef]
8. Ma, X.L.; Jiao, Q.; Kecskes, J.L.; El-Awady, J.A.; Weihs, T.P. Effect of basal precipitates on extension twinning and pyramidal slip: A micro-mechanical and electron microscopy study of a Mg–Al binary alloy. *Acta Mater.* **2020**, *189*, 35–46. [CrossRef]
9. Zha, M.; Zhang, H.M.; Wang, C.; Wang, H.Y.; Zhang, E.B.; Jiang, Q.C. Prominent role of a high volume fraction of $Mg_{17}Al_{12}$ particles on tensile behaviors of rolled Mg–Al–Zn alloys. *J. Alloy. Compd.* **2017**, *728*, 682–693. [CrossRef]
10. Li, Y.K.; Zha, M.; Jia, H.L.; Wang, S.Q.; Zhang, H.M.; Ma, X.; Tian, T.; Ma, P.K.; Wang, H.Y. Tailoring bimodal grain structure of Mg–9Al–1Zn alloy for strength-ductility synergy: Co-regulating effect from coarse Al_2Y and submicron $Mg_{17}Al_{12}$ particles. *J. Magnes. Alloy.* **2021**, *9*, 1556–1566. [CrossRef]
11. Shi, G.L.; Zhang, K.; Li, X.G.; Li, Y.J.; Ma, M.L.; Yuan, J.W.; Zhang, H.J. Dislocation configuration evolution during extension twinning and its influence on precipitation behavior in AZ80 wrought magnesium alloy. *J. Magnes. Alloy.* **2021**. [CrossRef]
12. Shi, R.H.; Miao, J.S.; Luo, A.A. A new magnesium sheet alloy and its multi-stage homogenization for simultaneously improved ductility and strength at room temperature. *Scr. Mater.* **2019**, *171*, 92–97. [CrossRef]
13. Tolouie, E.; Jamaati, R. Effect of β–$Mg_{17}Al_{12}$ phase on microstructure, texture and mechanical properties of AZ91 alloy processed by asymmetric hot rolling. *Mat. Sci. Eng. A* **2018**, *738*, 81–89. [CrossRef]
14. Shi, R.H. Nonisothermal dissolution kinetics on $Mg_{17}Al_{12}$ intermetallic in Mg–Al alloys. *J. Magnes. Alloy.* **2021**. [CrossRef]
15. She, J.; Pan, F.; Zhang, J.; Tang, A.; Luo, S.; Yu, Z.; Song, K.; Rashad, M. Microstructure and mechanical properties of Mg–Al–Sn extruded alloys. *J. Alloy. Compd.* **2016**, *657*, 893–905. [CrossRef]
16. Liu, T.T.; Yang, Q.S.; Guo, N.; Lu, Y.; Song, B. Stability of twins in Mg alloys—A short review. *J. Magnes. Alloy.* **2020**, *8*, 66–77. [CrossRef]
17. Guo, F.L.; Feng, B.; Fu, S.W.; Xin, Y.C.; Xu, S.W.; Liu, Q. Microstructure and texture in an extruded Mg–Al–Ca–Mn flat-oval tube. *J. Magnes. Alloy.* **2017**, *5*, 13–19. [CrossRef]
18. Zhou, B.J.; Wang, L.Y.; Wang, J.H.; Maldar, A.; Zhu, G.M.; Jia, H.L.; Jin, P.P.; Zeng, X.Q.; Li, Y.J. Dislocation behavior in a polycrystalline Mg-Y alloy using multi-scale characterization and VPSC simulation. *J. Mater. Sci. Technol.* **2022**, *98*, 87–98. [CrossRef]
19. Zhao, L.Y.; Chapuis, A.; Xin, Y.C.; Liu, Q. VPSC-TDT modeling and texture characterization of the deformation of a Mg–3Al–1Zn plate. *J. Alloy. Compd.* **2017**, *710*, 159–165. [CrossRef]
20. Tam, K.J.; Vaughan, W.M.; Shen, L.M.; Knezevic, M.; Karaman, I.; Proust, G. Modelling the temperature and texture effects on the deformation mechanisms of magnesium alloy AZ31. *Int. J. Mech. Sci.* **2020**, *182*, 105717. [CrossRef]

21. Molinari, A.; Canova, G.R.; Ahzi, S. A Self-Consistent Approach of the Large Deformation Polycrystal Viscoplasticity. *Acta Metall. Mater.* **1987**, *35*, 2983–2994. [CrossRef]

22. Lebensohn, R.A.; Tome, C.N. A Self-Consistent Viscoplastic Model—Prediction of Rolling Textures of Anisotropic Polycrystals. *Mat. Sci. Eng. A* **1994**, *175*, 71–82. [CrossRef]

23. Lebensohn, R.A.; Tome, C.N.; Maudlin, P.J. A selfconsistent formulation for the prediction of the anisotropic behavior of viscoplastic polycrystals with voids. *J. Mech. Phys. Solids* **2004**, *52*, 249–278. [CrossRef]

24. Maldar, A.; Wang, L.Y.; Zhu, G.M.; Zeng, X.Q. Investigation of the alloying effect on deformation behavior in Mg by Visco-Plastic Self-Consistent modeling. *J. Magnes. Alloy.* **2020**, *8*, 210–218. [CrossRef]

25. Zhang, Y.; Huang, X.; Ma, Z.; Li, Y.; Guo, F.; Yang, J.; Ma, Y.; Hao, Y. The influences of Al content on the microstructure and mechanical properties of as-cast Mg-6Zn magnesium alloys. *Mat. Sci. Eng. A* **2017**, *686*, 93–101. [CrossRef]

26. Zecevic, M.; Knezevic, M.; McWilliams, B.; Lebensohn, R.A. Modeling of the thermo-mechanical response and texture evolution of WE43 Mg alloy in the dynamic recrystallization regime using a viscoplastic self-consistent formulation. *Int. J. Plasticity* **2020**, *130*, 102705. [CrossRef]

27. Tomasz, C.; Wojciech, Z.; Elżbieta, B. Study of the thermal stability of phases in the Mg-Al system. *J. Phase Equilib.* **2003**, *24*, 249–254.

28. Li, M.; Cheng, Y.; Zheng, Y.F.; Zhang, X.; Xi, T.F.; Wei, S.C. Plasma enhanced chemical vapor deposited silicon coatings on Mg alloy for biomedical application. *Surf. Coat. Technol.* **2013**, *228*, S262–S265. [CrossRef]

29. Yu, L.; Yan, H.G.; Chen, J.H.; Xia, W.J.; Su, B.; Song, M. Effects of solid solution elements on damping capacities of binary magnesium alloys. *Mat. Sci. Eng. A* **2020**, *772*, 138707. [CrossRef]

30. Zhou, S.; He, X.; Peng, P.; Liu, T.; Sheng, G.; Tang, A.; Pan, F. Achieving high yield strength and ductility in as-extruded Mg–0.5Sr alloy by high Mn-alloying. *Materials* **2020**, *13*, 4176. [CrossRef]

31. Zhao, J.; Jiang, B.; Yuan, Y.; Tang, A.T.; Sheng, H.R.; Yang, T.H.; Huang, G.S.; Zhang, D.F.; Pan, F.S. Influence of Zn addition on the microstructure, tensile properties and work-hardening behavior of Mg–1Gd alloy. *Mat. Sci. Eng. A* **2020**, *772*, 138779. [CrossRef]

32. She, J.; Zhou, S.B.; Peng, P.; Tang, A.T.; Wang, Y.; Pan, H.C.; Yang, C.L.; Pan, F.S. Improvement of strength-ductility balance by Mn addition in Mg–Ca extruded alloy. *Mat. Sci. Eng. A* **2020**, *772*, 138796. [CrossRef]

33. Zheng, X.; Du, W.; Liu, K.; Wang, Z.; Li, S. Effect of trace addition of al on microstructure, texture and tensile ductility of Mg–6Zn–0.5Er alloy. *J. Magnes. Alloy.* **2016**, *4*, 135–139. [CrossRef]

34. Yu, H.; Li, C.; Xin, Y.; Chapuis, A.; Huang, X.; Liu, Q. The mechanism for the high dependence of the Hall-Petch slope for twinning/slip on texture in Mg alloys. *Acta Mater.* **2017**, *128*, 313–326. [CrossRef]

35. Bakarian, P.W. *Glide and Twinning in Magnesium Single Crystals at Elevated Temperatures*; Yale University: New Haven, CT, USA, 1941.

36. Akhtar, A.; Teghtsoonian, E.J.A.M. Solid solution strengthening of magnesium single crystals—ii the effect of solute on the ease of prismatic slip. *Acta Metall.* **1969**, *17*, 1351–1356. [CrossRef]